

Oligo- and Polymeric Pd^{II} and Pt^{II} Using Pyridyl Carboxylate Spacers for Topology Control

Peili Teo, L. L. Koh, and T. S. Andy Hor*

Department of Chemistry, National University of Singapore, 3 Science Drive 3, Singapore 117543, Singapore

Received April 23, 2008

An array of Pd^{II} and Pt^{II} supramolecular assemblies have been constructed using pyridyl carboxylates as spacers and phosphines [(C₅H₄PPh₂)₂Fe (dppf) and PPh₃] as supporting ligands. Different molecular topologies such as squares, triangles, rectangles, and polymers can be controlled by the spatial and directional character of the spacer. A change of the denticity of the phosphine does not affect the topological outcome. Significant differences, however, are observed for the congeneric analogues, with Pd^{II} showing a more pronounced tendency toward coordination polymer formation and its attached carboxyl a higher affinity toward Ag⁺. The ability of these assemblies to capture cations, such as Na⁺ in [Pt₃Na(3-NC₅H₄CO₂)₃(OTf)₃(PPh₃)₆]⁺ through hydrogen bonding or Ag⁺ in [PdAg(2-NC₅H₄CO₂)(OTf)₂(dppf)] through dative bonding, is described and compared. All of the complexes are structurally characterized by single-crystal X-ray crystallography.

Introduction

The science of “coordination assembly” is rapidly developing into a fascinating field in which a variety of supramolecular architectures are constructed using different methodologies. A key challenge in such a molecular assembly process is to direct an essentially thermodynamically driven process to the desirable target. In the area of metal-based assemblies, this requires coordination, geometric, structural, and topological manipulations. The success of such control often determines the functional value of the resultant materials in areas such as catalysis, separation and purification, energy storage, drug delivery, polymerization, as well as electronic devices. There are emerging examples that highlight the different strategies that are being developed. Our focus in this area is on the complementary use of directional spacers and geometrically defined metals to prepare small polygons with functional value. Recent reports on the use of d⁸ and d¹⁰ metals with spacers such as diphosphines, thiophenes, and hybrid ligands such as pyridyl carboxylates are examples of our approaches. In this paper, we demonstrate how specific topological outcomes can be achieved through the combinative use of planar metals as well as directionally specific and heterodonating spacers such as pyridyl carboxylates. This is illustrated by the isolation

and structural elucidation of a range of coordination assemblies that are systematically constructed by tuning the relative orientation and separation of the donor functionalities. The results suggested that, given the appropriate choice of metals and spacers, self-assemblies can indeed give predictive outcomes at both molecular and crystal structural levels.

Results and Discussion

We use inert square-planar d⁸ metals (Pd^{II} and Pt^{II}) with two neighboring sites blocked by a chelating diphosphine [Fe(C₅H₄PPh₂)₂, 1,1'-bis(diphenylphosphino)ferrocene (dppf)] or two monophosphines (PPh₃) to ensure planar and cis propagation. Pyridyl carboxylates [NC₅H₄(CH₂)_nCO₂⁻] are chosen because they have two stable donor atoms for d⁸ metals and the directional links can be adjusted to ~180°, 120°, or 60° depending on para, meta, or ortho substitution. Control of the connecting CH₂ unit provides a means to manipulate the internal angles of the polygon and its cavity size. These simple tools are self-sufficient to construct coordination squares, triangles, rectangles, polymers, and their basic building block of mononuclear metalloligands. A summary of all of the complexes described in this paper is given in Table 1.

A molecular square is relatively easy to assemble. Similar success was reported earlier.^{3a} The inherent square-planar geometry of d⁸ metals makes these ideal corners for squares.

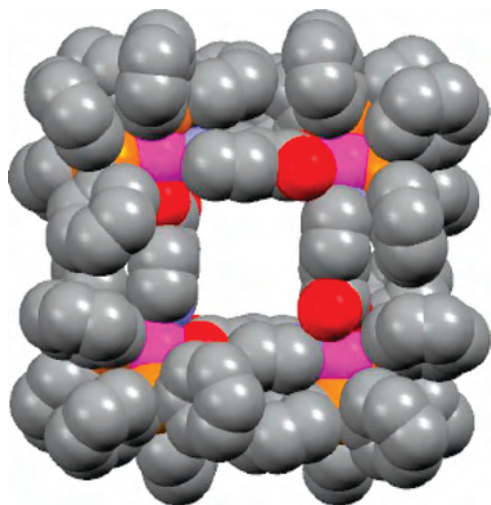
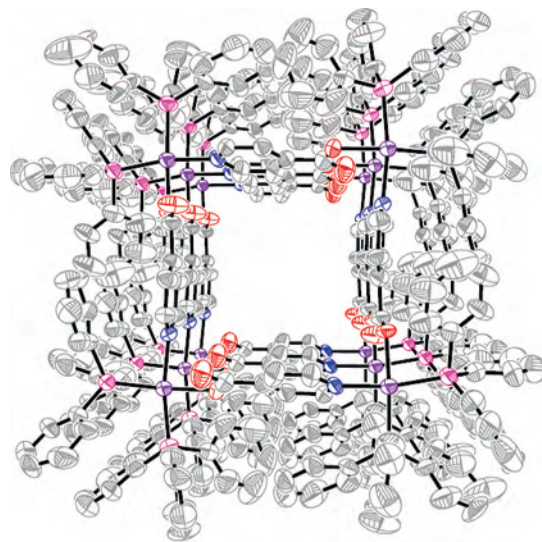
* To whom correspondence should be addressed. E-mail: andyhor@nus.edu.sg. Tel: 65 65162679. Fax: 65 65162663.

Table 1. Summary of Topological Outcomes in the Self-Assembly between Pd^{II} or Pt^{II} with a Representative Series of Pyridyl Carboxylates Supported by dppf or PPh₃^a

	Pt ^{II} (PPh ₃) ₂	Pt ^{II} dppf ^a	Pd ^{II} dppf ^a
4-pyridylformate (isonic)	square, 1a	square	polymer, 1b
3-pyridylformate (Nic ^a)	triangle, 4c	triangle, 4b	triangle, 4a
2-pyridylformate (Pic ^a)	mononuclear, 6d	mononuclear, 6c	mononuclear, 6b
4-pyridylacetate (PyOAc)	rectangle, 5	rectangle	rectangle
4-pyridylbenzoate (PyPhCO ₂)	decomposed	mononuclear, 7d	mononuclear, 7b
4-pyridylacrylate (PyAcr)	decomposed	mononuclear, 3	polymer, 2a

^a Nic = nicotinate; Pic = picolinate; dppf = 1,1'-bis(diphenylphosphino)ferrocene.

A para orientation of the donors and their short separation (viz., $n = 0$) would best equip such spacers to serve as the square edges. This is demonstrated by the formation of [Pt(isonic)(PPh₃)₂]₄(OTf)₄ (**1a**; Figure 1) from [Pt(PPh₃)₂(MeCN)₂]²⁺, and isonicotinic acid (isonicH, 4-pyridylformic acid) with a square cavity of $\sim 5.6 \times 5.6 \text{ \AA}^2$, deducting the van der Waals radii. The reported dppf analogue also shows a similar cavity size.^{3a} Cavities of similar sizes have been found to host small molecules such as C₂H₂ or H₂. From the packing diagram of the [Pt(isonic)(PPh₃)₂]₄⁴⁺ square, it can be seen that the squares stack directly on top of one another, giving a square tunnel of cross-sectional area determined by the cavity size (Figure 2). The supporting phosphines serve to block the corners from further aggregation but do not influence the topology choice. Similar to the earlier reported [Pt(isonic)(dppf)]₄⁴⁺ analogue, the isonic ligand is N,O-heterocoordinated at the same metal center. However, the room temperature ³¹P{¹H} NMR spectrum of **1a** shows four doublets (δ 7.2, 6.8, 5.7, and 4.7 ppm), instead of two, as is expected from the solid-state structure (described below) and as is observed in the NMR spectrum of the dppf analogue.^{3a} At 233 K, one of the pairs of doublets diminishes in intensity and virtually disappears at lower temperatures, leaving behind the pair whose chemical shifts (δ 7.5 and 6.8 ppm) are comparable to those of other Pt^{II}(PPh₃)₂ pyridylcarboxylate

**Figure 1.** Space-filling model of **1a**, showing a square cavity at the center.**Figure 2.** ORTEP drawing (50% thermal ellipsoids) of **1a**, showing the molecular stacking of the squares to give a tubular crystal structure in the solid-state packing diagram. (H atoms and anions are omitted for clarity.)

complexes. These changes are reversible over the temperature range of the experiments. They point to two dynamic isomers in solution, one of which, probably the one that persists throughout the temperature range, corresponds to that of the solid-state structure (**1a**) while the other remains unknown. The sample gave reproducible spectra upon prolonged storage (within 1 year). The ²J_{P-P} (22.3 Hz) and J_{P-Pt} (4276 and 3539 Hz) couplings are within expectations. The ¹H NMR spectrum of **1a** reveals the characteristic pyridyl protons [(δ 8.4 (s) and 8.2 (s) ppm], whereas the IR spectrum gives C=O stretches {1638 [$\nu_{\text{asym}}(\text{COO})$] and 1261 [$\nu_{\text{sym}}(\text{COO})$] cm⁻¹} similar to those of the dppf analogue.

The most likely side product in a square construction is the coordination polymer because they share similar basic formation criteria. This is illustrated by the isolation of **1b** from [Pd(dppf)(MeCN)₂]²⁺ and isonicH as a straight-chain zigzag polymer (Figure 3). The alternating N,O heterocoordination gives a ³¹P NMR fingerprint for the differentiation of the *trans*-phosphines (δ 34.3 and 39.0 ppm). ESI-MS analysis gives the [Pd(isonic)(dppf)]⁺ ion peak at $m/z = 783.91$.

A more reliable means to producing coordination polymers in this system is to use an extended spacer but maintaining the linear directionality. This is achieved by the use of

- (1) (a) Higuchi, M.; Horike, S.; Kitagawa, S. *Supramol. Chem.* **2007**, *19*, 75. (b) Yamada, K.; Yagishita, S.; Tanaka, H.; Tohyama, K.; Adachi, K.; Kaizaki, S.; Kumagai, H.; Inoue, K.; Kitaura, R.; Chang, H.; Kitagawa, S.; Kawata, S. *Chem.—Eur. J.* **2004**, *10*, 2647. (c) Cairns, A. J.; Perman, J. A.; Wojtas, J.; Kravtsov, V. C.; Alkordi, M. H.; Eddaoudi, M.; Zawarotko, M. J. *J. Am. Chem. Soc.* **2008**, *130*, 1560. (d) Lehn, J.-M. *Supramolecular Chemistry—Concepts and Perspectives*; VCH: Weinheim, Germany, 1995. (e) *Comprehensive Supramolecular Chemistry*; Atwood, J. L., Davies, J. E. D., MacNicol, D. D., Vogtle, F., Lehn, J.-M., Eds.; Pergamon: Oxford, U.K., 1996; Vol. 9. (f) Ward, M. D. *Annu. Rep. Prog. Chem., Sect. A* **2000**, *96*, 345. (g) Cheetham, A. K.; Rao, C. N. R.; Feller, R. K. *Chem. Commun.* **2006**, 4780. (h) Leininger, S.; Olenyuk, B.; Stang, P. J. *Chem. Rev.* **2000**, *100*, 3483. (i) Stang, P. J.; Olenyuk, B. *Acc. Chem. Res.* **1997**, *30*, 502. (j) Vriezma, D. A.; Argones, M. C.; Elemans, J. A. A. W.; Cornelissen, J. J. L. M.; Rowan, A. E.; Nolte, R. J. M. *Chem. Rev.* **2005**, *105*, 1445.

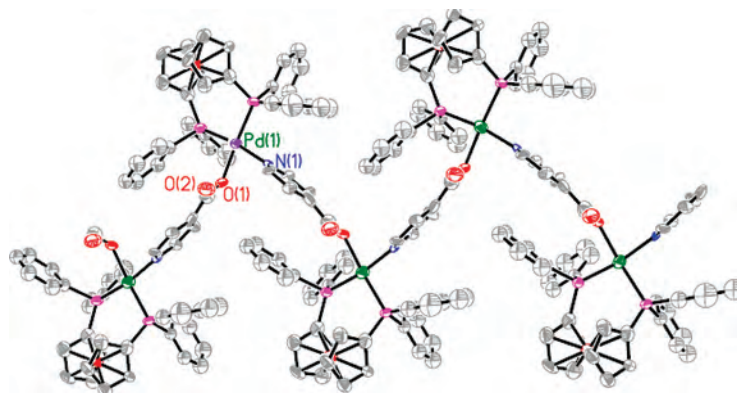


Figure 3. ORTEP drawing of **1b**, showing a zigzag coordination polymer. (H atoms omitted for clarity.)

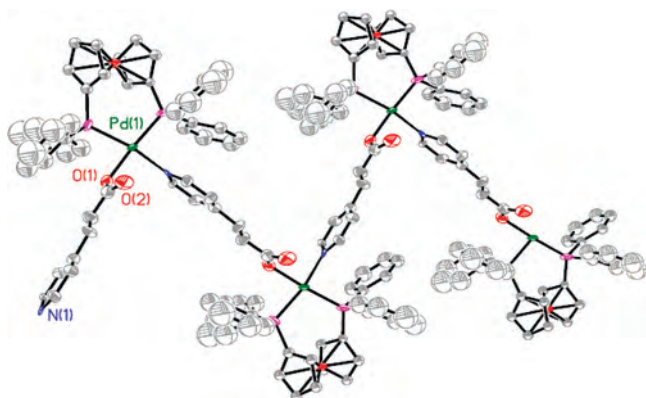


Figure 4. ORTEP drawing of **2a**, showing a zigzag coordination polymer. (H atoms omitted for clarity.)

4-pyridylacrylic acid (PyAcrH), which has a connecting C=C moiety, as shown in the formation of $[\text{Pd}(\text{PyAcr})(\text{dppf})]_n(\text{OTf})_n$ (**2a**; Figure 4). In both **1b** and **2a** (Table 2), the zigzag unidirectional propagation is ensured when the two cis sites of the planar metal are blocked by the diphosphine. Such a coordination polymer is relatively uncommon, especially among the crystallographically established systems, compared to rings and cages, because they are entropically less favorable and their general insolubility makes characterization difficult. There is no evidence for the formation of the analogous Pd_4 square or other nuclearity isomers; the polymer form appears to be the thermodynamic sink. The reaction of $[\text{Pt}(\text{dppf})(\text{MeCN})_2]^{2+}$ with PyAcrH leads to the isolation of a solid whose ^{31}P NMR spectrum shows a mixture of an N,O-ligated complex $[\text{Pt}(\text{PyAcr})(\text{dppf})]_n(\text{OTf})_n$ (**2b**) [δ 8.1 ppm ($J_{\text{P-Pt}} = 3781$ Hz); δ 5.7 ppm ($J_{\text{P-Pt}} = 3488$ Hz); $^2J_{\text{P-P}} = 17.4$ Hz] and an N-only complex $[\text{Pt}(\text{PyAcrH})_2(\text{dppf})](\text{OTf})_2$ (**3**) [δ 4.6 ppm ($J_{\text{P-Pt}} = 3369$ Hz)] (Figure 5 and Table 3). The spectrum of the *in situ* reaction mixture gives the latter as the main kinetic species. It steadily gives rise to the enthalpic product upon concentration of the

reaction solutions. This conversion is assisted by trifluoromethanesulfonic or triflic acid (HOTf) elimination. Upon removal of solvents, a mixture of both the N-only complex (minor) and the N,O-ligated complex (major) is obtained. The mixture can be separated by anion exchange with NH_4PF_6 . However, poor solubility of **2b** upon anion exchange precluded it from recrystallization or crystallographic characterization.

d^8 metals are generally not tuned for molecular triangles because their coordination angles ($\sim 90^\circ$) are too big for the ideal internal angles (60°) of a triangle. This problem can be overcome by using a meta-substituted carboxylate with a short spacer ($n = 0$), viz., nicotinic acid (NicH, 3-pyridylformic acid), which provides the necessary wedges to fit the metals into the corners without compromising their natural geometries. This is illustrated by the assembly of $[\text{Pd}(\text{Nic})(\text{dppf})]_3(\text{OTf})_3$ (**4a**), $[\text{Pt}(\text{Nic})(\text{dppf})]_3(\text{OTf})_3$ (**4b**), and $[\text{Pt}(\text{Nic})(\text{PPh}_3)_2]_3(\text{OTf})_3$ (**4c**) (Figure 6 and Tables 4 and 5) from their MeCN-solvento precursors and NicH (nicotinic or 3-pyridylformic acid).

A particularly notable feature of the triangular construction is that the pendant carbonyl O atom is stereochemically confined to point upward and toward the center of the topological cavity in a clawlike fashion. This enables the entrapment of acidic entities through hydrogen bonding. For example, the cavity of both **4a** and **4b** traps CHCl_3 via weak hydrogen bonding between the carbonyl O atom and CHCl_3 H atom ($\text{O}\cdots\text{H}$ ave 2.559 Å for **4a**), giving CHCl_3 channels in the crystal lattice. Ghosh et al. recently reported the structure of **4a**, but there is no apparent convergence of the carbonyls in the triangle and hence no solvent trapping capability is mentioned. The difference may be attributed to the different solvents used in the preparation of **4a**; a highly polar methanolic environment was used in the report, as compared to the less polar CH_2Cl_2 favored by us. Complex **4c** crystallizes by capturing adventitious Na^+ , possibly

Table 2. Selected Bond Lengths and Angles for **1b** and **2a**

bond length/Å	1b	2a	bond angle/deg	1b	2a
Pd(1)–N(1)	2.105(7)	2.076(5)	N(1)–Pd(1)–O(1)	87.1(3)	85.3(3)
Pd(1)–O(1)	2.081(6)	2.061(11)	N(1)–Pd(1)–P(1)	92.4(2)	89.9(2)
Pd(1)–P(1)	2.262(2)	2.277(4)	N(1)–Pd(1)–P(2)	168.6(2)	169.3(2)
Pd(1)–P(2)	2.288(3)	2.273(4)	P(2)–Pd(1)–P(1)	97.89(9)	100.14(10)
C(1)–O(1)	1.282(11)	1.30(2)	O(1)–Pd(1)–P(1)	178.0(2)	173.8(4)
C(1)–O(2)	1.213(11)	1.18(2)	O(1)–Pd(1)–P(2)	82.44(18)	84.4(3)

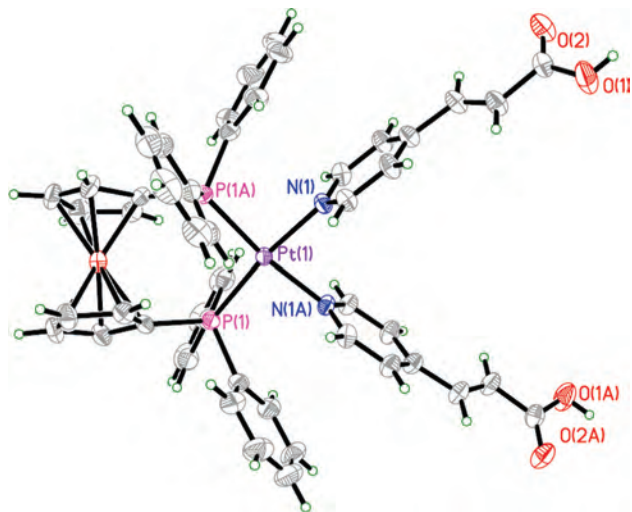


Figure 5. ORTEP drawing of **3**, showing the N-only coordination of the pyridyl carboxylate ligands.

Table 3. Selected Bond Lengths and Angles for **3**

Bond Length/Å	
Pt(1)–N(1)	2.090(2)
Bond Angles/deg	
N(1)#1–Pt(1)–N(1)	83.19(13)
N(1)#1–Pt(1)–P(1)#1	171.26(6)
N(1)–Pt(1)–P(1)#1	88.24(7)
N(1)#–Pt(1)–P(1)	88.24(7)
N(1)–Pt(1)–P(1)	171.26(6)
P(1)–Pt(1)–P(1)#1	100.36(4)

leached from the celite used in filtration, by its carbonyl claws to give Na[(Na(H₂O)₃(OTf)₃)]C**4c**(OTf)₂, through strong hydrogen bonding (O⋯H ~ 1.321 Å; Figure 7). Its crystal lattice reveals triangular-shaped channels. Each octahedral [Na(OTf)₃(H₂O)₃]²⁺ is sandwiched by the triangular complexes and juxtaposed along the triangular pore by hydrogen bonding.

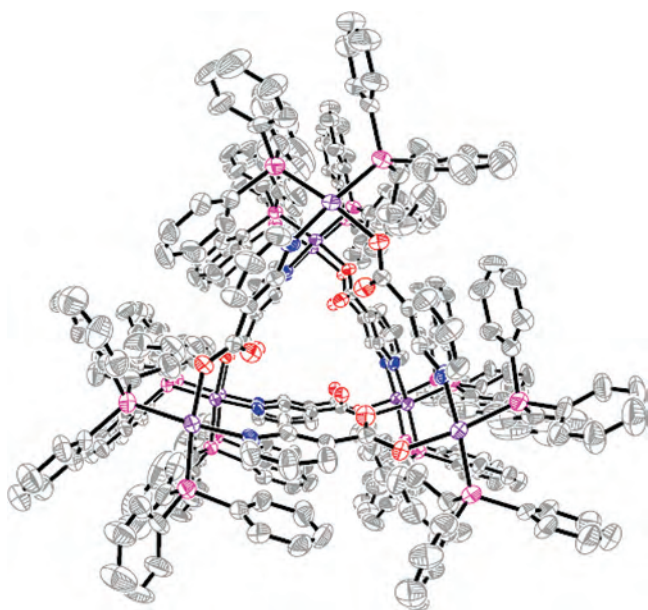


Figure 6. ORTEP drawing of **4c**, showing three molecular triangles stacked on top of each other. (H atoms are omitted for clarity.) Structures **4a–c** are isostructural.

Table 4. Selected Bond Lengths for Complexes **4a–c**

bond length/Å	4a	4b	4c
Pt(1)–N(1)/Pd(1)–N(1)	2.087(13)	2.085(11)	2.082(5)
Pt(1)–O(1)/Pd(1)–O(1)	2.084(11)	2.089(10)	2.094(6)
Pt(2)–N(2)/Pd(2)–N(2)	2.102(13)	2.087(12)	
Pt(2)–O(2)/Pd(2)–O(2)	2.087(12)	2.089(10)	
Pt(3)–N(3)/Pd(3)–N(3)	2.090(14)	2.085(12)	
Pt(3)–O(3)/Pd(3)–O(3)	2.080(11)	2.090(10)	
C(6)–O(3)	1.24(2)	1.298(18)	1.286(9)
C(6)–O(4)	1.246(19)	1.210(19)	1.216(10)
C(12)–O(5)	1.29(2)	1.290(17)	
C(12)–O(6)	1.22(2)	1.229(17)	
C(18)–O(1)	1.224(19)	1.276(18)	
C(18)–O(2)	1.251(18)	1.209(17)	

Table 5. Selected Bond Angles for Complexes **4a–c**^a

bond angle/deg	4a	4b	4c
O(1)–Pd(1)–N(1)/O(1)–Pt(1)–N(1)	88.9(5)	87.7(4)	83.9(2)
O(3)–Pd(2)–N(2)/O(3)–Pt(2)–N(2)	86.6(5)	84.7(5)	
O(5)–Pd(3)–N(3)/O(5)–Pt(3)–N(3)	86.9(5)	85.9(5)	

^a For **4c**, because of *P6(3)/m* symmetry, only one set of bond data are needed, and it is labeled as Pt(1)–N(1), Pt(1)–O(1), and O(2)=C(1)–O(1) in the structure.

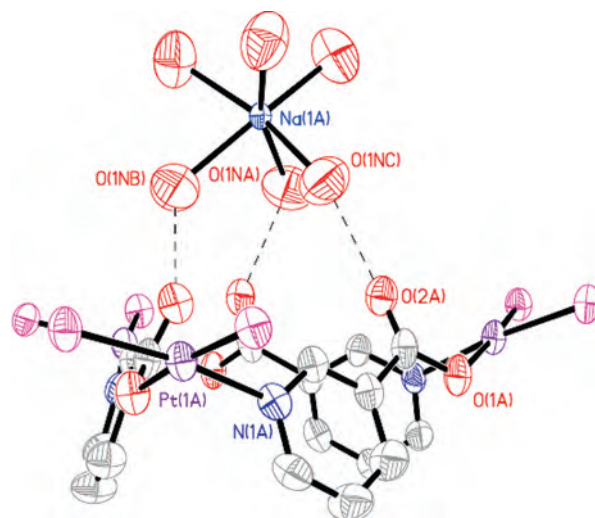


Figure 7. ORTEP drawing of **4c**, showing the triangular core with the C=O “claws” pointing upward and coordinated to the hydrated Na⁺. The bottom three O atoms are that of H₂O, whereas the top three are triflate O atoms. The H atoms could not be located because of the unsatisfactory data quality. The hydrogen bonding is estimated based on the short O separation of 2.642 Å.

obtained when NaOTf is added to the reaction solution of [Pt(PPh₃)₂(MeCN)₂]²⁺ and NiCH, in stoichiometric amounts. On the other hand, the complex cannot be prepared without Na⁺ because the framework collapses easily without Na⁺ as a template.

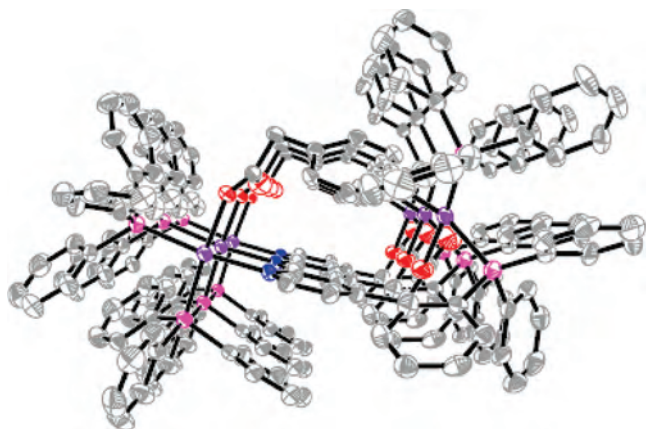
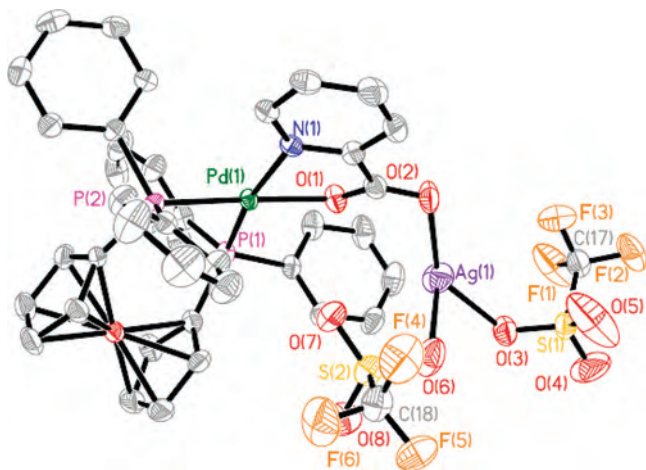
A molecular rectangle-like topology can be achieved through the introduction of a connector, i.e., *n* = 1. This is witnessed in the formation of [Pt(PyOAc)(PPh₃)₂]₂(OTf)₂ (**5**; Table 6) from [Pt(PPh₃)₂(MeCN)₂]²⁺ and PyOAcH (4-pyridylacetic acid). The resultant dinuclear frame features two metal and two CH₂ corners connected by two long pyridyls and two short carboxyls, giving a rectangle-like polygon. The molecules stack up neatly to give a rectangular channel with a cross-sectional area of ~3.0 × 1.1 Å², excluding van der Waals radii (Figure 8). A similar assembly was obtained with the reported Pt^{II}- and Pd^{II}dppf PyOAc complexes.^{3b,c} The connecting CH₂ relaxes the dimensional

Table 6. Selected Bond Lengths and Angles for Complexes **1a** and **5**

bond length/Å	1a	5	bond angle/deg		
Pt(1)–N(1)	2.068(8)	2.077(4)	N(1)–Pt(1)–O(3)	85.0(3)	85.02(14)
Pt(1)–O(1)	2.071(6)	2.078(3)	N(1)–Pt(1)–P(1)	91.8(2)	169.71(11)
Pt(2)–N(2)	2.107(8)	2.103(4)	O(3)–Pt(1)–P(1)	176.8(2)	85.64(10)
Pt(2)–O(2)	2.099(7)	2.058(4)	N(1)–Pt(1)–P(2)	169.9(2)	91.37(11)
Pt(1)–P(1)	2.250(3)	2.2740(13)	O(3)–Pt(1)–P(2)	85.1(2)	175.72(10)
Pt(1)–P(2)	2.277(3)	2.2492(13)	N(2)–Pt(2)–O(1)	85.8(3)	83.98(15)
Pt(2)–P(3)	2.279(3)	2.2418(13)	N(2)–Pt(2)–P(4)	89.6(2)	165.38(11)
Pt(2)–P(4)	2.251(3)	2.2779(14)	O(1)–Pt(2)–P(4)	173.9(2)	84.38(12)
			N(2)–Pt(2)–P(3)	167.8(2)	92.70(11)
			O(1)–Pt(2)–P(3)	85.8(2)	174.44(13)

rigidity of a linear spacer such as isonic. In the Pd^{II}dppf systems, the pendant carbonyl captures acidic Ag^I, leading to the formation of heterometallic assemblies.

Ortho-substituted pyridyls cannot give polygons but mononuclear chelating complexes because of the proximity of the heterodonors. The formation of [Pd(Pic)(dppf)](OTf) (**6a**) from [Pd(dppf)(MeCN)₂]²⁺ and PicH (picolinic acid, or 2-pyridylformic acid) is an example. Such species are potential metalloligands for heterometallic polygon assemblies. This is illustrated by the ability of the pendant carbonyl to attract an acidic metal moiety such as AgOTf. The X-ray crystallographic structure of [PdAg(Pic)(OTf)₂(dppf)] (**6b**; Figure 9 and Table 7) shows the resultant assembly in which the trigonal-planar Ag^I is stabilized by

**Figure 8.** ORTEP drawing showing the molecular stacks of **5** to give a rectangle-like tunnel. (H atoms are omitted for clarity.)**Figure 9.** ORTEP drawing of **6b**, showing the attraction of Ag⁺ to the pendant carbonyl. (H atoms are omitted for clarity.)

the carbonyl and two triflates [Ag–O 2.275(5) Å]. The ³¹P{¹H} NMR spectrum of **6b** also shows two broad resonances ($\nu_{1/2} \sim 100$ Hz). The two phosphine signals are significantly shifted downfield as compared to that in **1b** and **4a** (**6b**, δ 42.5 and 39.5 ppm; **1b**, δ 39.0 and 34.3 ppm; **4a**, δ 39.0 and 33.6 ppm). The deshielding is a possible result of the coordination of the acidic [Ag(OTf)₂][–] group to the carbonyl of the Pic ligand at the trans position. This coordination also weakens the C=O bond, as is evident from the red shift of the symmetric carbonyl stretch in the IR spectrum when compared to the metalloligand **6a** [ν 1625 [$\nu_{\text{asym}}(\text{COO})$], 1262 [$\nu_{\text{sym}}(\text{COO})$] cm^{–1} for **6a**; ν 1655 [$\nu_{\text{asym}}(\text{COO})$], 1164 [$\nu_{\text{sym}}(\text{COO})$] cm^{–1} for **6b**]. The C=O bond length in **6b** is also significantly longer than that in **1b** but comparable to that in **4a**, which shows hydrogen bonding with CHCl₃ [C=O 1.229(7) Å for **6b**; ave 1.23 Å for **4a**; 1.213(11) Å for **1b**]. Pure **6b** cannot be isolated because it is inevitably contaminated by **6a**, even when a large excess of AgOTf is used in the preparation of **6b**. Complete separation of the mixture was unsuccessful because of the hygroscopic nature of **6b**. Complex **6a**, however, could be obtained pure from the reaction of [Pd(dppf)(MeCN)₂]²⁺, generated in situ from a stoichiometric mixture of PdCl₂(dppf) and AgOTf, with PicH. The Pt^{II} analogue of **6a**, viz., [Pt(Pic)(dppf)](OTf) (**6c**), can be prepared from the ligand exchange of [Pt(dppf)(MeCN)₂]²⁺ with PicH. Similarly, [Pt(Pic)(PPh₃)₂]OTf (**6d**) can be prepared. Because these complexes show no affinity toward Ag^I, even in a large excess of AgOTf, it provides a general distinguishing feature between the Pd^{II} and Pt^{II} metalloligands.

It is generally difficult to prepare metalloligand precursors with an extended spacer because of the heavily favored thermodynamic (enthalpy) gains from coordination, leading

Table 7. Selected Bond Lengths and Angles for Complexes **6b–d**

	6b	6c	6d
Bond Length/Å			
Pt(1)–N(1)/Pd(1)–N(1)	2.131(4)	2.122(3)	2.110(3)
Pt(1)–O(1)/Pd(1)–O(1)	2.065(4)	2.052(3)	2.043(2)
C(6)–O(1)	1.276(7)	1.302(6)	1.295(4)
C(6)–O(2)	1.229(7)	1.224(5)	1.217(4)
Ag(1)–O(2)	2.275(5)		
Ag(1)–O(3)	2.402(5)		
Ag(1)–O(6)	2.470(5)		
Bond Angle/deg			
O(1)–Pd(1)–N(1)/O(1)–Pt(1)–N(1)	78.90(17)	79.71(12)	79.86(10)
O(2)–Ag(1)–O(3)	143.19(16)		
O(2)–Ag(1)–O(6)	97.1(2)		
O(3)–Ag(1)–O(6)	93.47(18)		
O(1)–Pd(1)–N(1)/O(1)–Pt(1)–N(1)	78.90(17)	79.71(12)	79.86(10)

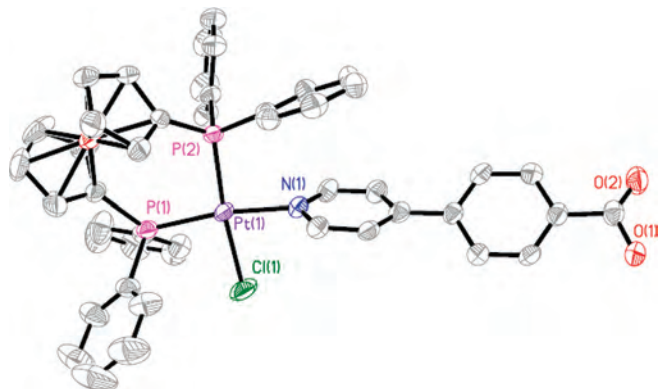


Figure 10. ORTEP drawing of **7d**, showing a potential metalloligand with heterofunctional ligands. (H atoms are omitted for clarity.)

to polygons or polymers. This can be overcome in the current system by a destructive method in which a preformed polymer is decomposed by the use of a reactive solvent. The construction of [PdCl(PyPhCO₂H)(dppf)]OTf (**7b**) from [Pd(dppf)(MeCN)₂]²⁺ and PyPhCO₂H (4-pyridylbenzoic acid) via [Pd(PyPhCO₂)(dppf)_n(OTf)_n (**7a**; δ(³¹P) 33.7 and 36.3 ppm) with CH₂Cl₂ illustrates this approach. The same method can be applied to [PtCl(PyPhCO₂H)(dppf)]OTf (**7d**; Figure 10 and Table 8) from [Pt(dppf)(MeCN)₂]²⁺ and PyPhCO₂H via [Pt(PyPhCO₂)(dppf)₄(OTf)₄ (**7c**). The destruction of **7c** enables Pt^{II} to capture Cl⁻ from the solvent (CHCl₃) and form a stable mononuclear species. Complexes **7b** and **7d** are potential precursors for heterometallic polygons and polymers, which are relatively rare. Its para-directing carboxyl and benzyl connectors would minimize any conflicts between metals. Its pendant carboxyl, which is usually too reactive to be isolated, is stabilized by protonation to give a carboxylic acid. Pyridylbenzoates as spacers with coordinating carboxylate functions are known.^{4a} A similar phenomenon is observed in **3**. The PPh₃ analogues of **7c** and **7d** are too unstable to be isolated.

The structural outcomes of these assemblies are summarized in Table 1. There is no concrete evidence to suggest that the solid-state structures of supramolecules are maintained in solutions because their solution spectroscopic data are generally not structurally diagnostic. There is, however, collective proof that a careful choice of spacers and metals can result in a high level of precision in this form of predictive self-assemblies of supramolecules. The consistent

and common assemblies between Pt^{II} and Pd^{II} and between diphosphines and monophosphines point to the dominant influence of the spacer on the topological outcome. At least within this system, we have a convenient and reliable mechanism to control the topology, cavity size, and ionic and molecular entrapment (Table 9 and Schemes 1 and 2). The carbonyls in the Pd^{II} complexes appear to be more basic and, hence, more receptive to adventitious Ag⁺. The [Pt^{II}(PPh₃)₂] triangle is highly sensitive to Na⁺ even in very low concentrations. This has encouraged us to develop these supramolecules as selective metal sensors. Current work in our laboratory is directed at these initiatives.

Experimental Section

General Procedures. All reactions were performed under pure dry nitrogen using standard Schlenk techniques. The products are air-stable, and hence recrystallizations were performed in air. All chemicals used in the synthesis were of reagent-grade-quality obtained from commercial sources and used as received. Commercial reagents MeCN, CH₂Cl₂, and CHCl₃ were predried using a commercial solvent drier, and PtCl₂(dppf), PdCl₂(dppf), and *cis*-PtCl₂(PPh₃)₂ were prepared as reported. [Pt(dppf)(MeCN)₂](OTf)₂, [Pd(dppf)(MeCN)₂]²⁺, and [Pt(PPh₃)₂(MeCN)₂]²⁺ were also prepared according to literature procedures.^{3,9}

All ¹H NMR [δ(TMS) 0.0 ppm] and ³¹P{¹H} NMR [δ(85% H₃PO₄) 0.0 ppm] were recorded at ca. 300 K at operating frequencies of 500.13 and 202.45 MHz, respectively, on a Bruker AVANCE 500 MHz spectrometer. Elemental analyses were performed by the Elemental Analysis Laboratory of our department. Electrospray ionization mass spectrometry spectra were obtained with a Finnigan/MAT LCQ mass spectrometer coupled with a TSP4000 HPLC system and the crystal 310 CE system. Samples were injected via a Rheodyne valve fitted with a 5 μL sample loop. The capillary temperature was uniformly set at 70 °C for obtaining of the spectra. Peak identifications were based on the *m/z* values and the isotopic distribution patterns. The *m/z* values given are for the most intense peak in the envelopment in each case. Samples used for elemental analyses were generally obtained directly from purified samples but may not be the single crystals used for single-crystal X-ray diffraction studies.

Syntheses. Synthesis of [Pt(isonic)(PPh₃)₂]₄(OTf)₄ (1a**).** To an aliquot of [Pt(PPh₃)₂(MeCN)₂]²⁺ was added isonicH (0.0092 g, 0.075 mmol), and the mixture was stirred for 5 h. The mixture was filtered and the filtrate concentrated to ca. 3 mL. Et₂O was added to afford a white precipitate in 72% (0.054 g) yield. ³¹P{¹H} NMR: δ 7.5 (d; *J*_{P-Pt} = 4276 Hz), 6.8 (d; *J*_{P-Pt} = 3539 Hz, ²*J*_{P-P} = 22.3 Hz) ppm. ¹H NMR: δ 8.4, 8.2 (s; pyridyl H), 6.7–7.4 (m; phenyl H) ppm. ESIMS: *m/z* (%) 877.76 (100) ([PtCl(PPh₃)₂-(isonicH)]⁺), 841.7 (20) ([Pt(isonic)(PPh₃)₂]⁺). IR (KBr): ν 1638 [ν_{asym}(COO)], 1261 [ν_{sym}(COO)] cm⁻¹. Anal. Calcd for **1a**·3CHCl₃: C, 48.64; H, 3.24; N, 1.30. Found: C, 48.30; H, 3.53; N, 1.38.

Synthesis of [Pd(isonic)(dppf)_n(OTf)_n (1b**).** To an aliquot of [Pd(dppf)(MeCN)₂]²⁺ in 20 mL of a CH₃CN/CH₂Cl₂ mixture was added isonicH (0.0185 g, 0.15 mmol), and the mixture was stirred for 5 h. The mixture was then filtered and the filtrate concentrated to ca. 3 mL. Et₂O was added to afford a pink precipitate in 85% (0.052 g) yield. ³¹P{¹H} NMR: δ 34.3 (b), 39.0 (b) ppm. ¹H NMR:

(2) (a) Matsuda, R.; Kitaura, R.; Kitagawa, S.; Kubota, Y.; Belosludov, R. V.; Kobayashi, T. C.; Sakamoto, H.; Chiba, T.; Takata, M.; Kawazoe, Y.; Mita, Y. *Nature* **2005**, *436*, 238. (b) Zhang, J.-P.; Kitagawa, S. *J. Am. Chem. Soc.* **2008**, *130*, 907. (c) Yaghi, O. M.; O'Keaffe, M.; Ockwig, N. W.; Chae, H. K.; Eddaoudi, M.; Kim, J. *Nature* **2003**, *423*, 705. (d) Moulton, B.; Zawarotko, M. J. *Chem. Rev.* **2001**, *101*, 1629. (e) Sato, S.; Lita, J.; Suzuki, K.; Kawano, M.; Ozeki, T.; Fujita, M. *Science* **2006**, *313*, 1273. (f) Fiedler, D.; Leung, D. H.; Bergman, R. G.; Raymond, K. N. *J. Am. Chem. Soc.* **2004**, *126*, 3674. (g) Credi, A. *Angew. Chem., Int. Ed.* **2007**, *46*, 5472. (h) Bera, J. K.; Bacsá, J.; Smucker, B. W.; Dunbar, K. R. *Eur. J. Inorg. Chem.* **2004**, 368. (i) Wong, K. M.; Hung, L.; Lam, W. H.; Zhu, N.; Yam, V. W. *J. Am. Chem. Soc.* **2007**, *129*, 4350. (j) You, C.; Würthner, F. *J. Am. Chem. Soc.* **2003**, *125*, 9716. (k) Shimomura, S.; Horike, S.; Matsuda, R.; Kitagawa, S. *J. Am. Chem. Soc.* **2007**, *129*, 10990. (l) Horike, S.; Bureekaew, S.; Kitagawa, S. *Chem. Commun.* **2008**, 471. (m) Fujita, M.; Tominaga, M.; Hori, A.; Therien, B. *Acc. Chem. Res.* **2005**, *38*, 371. (n) Fujita, M.; Yazaki, J.; Ogura, K. *J. Am. Chem. Soc.* **1990**, *112*, 5645.

(3) (a) Teo, P.; Koh, L. L.; Hor, T. S. *Inorg. Chem.* **2003**, *42*, 7290. (b) Teo, P.; Foo, D. M. J.; Koh, L. L.; Hor, T. S. *Dalton Trans.* **2004**, *20*, 3389. (c) Teo, P.; Koh, L. L.; Hor, T. S. *Inorg. Chim. Acta* **2006**, *359*, 3435. (d) Teo, P.; Koh, L. L.; Hor, T. S. *Chem. Commun.* **2007**, 2225.

Table 8. Selected Bond Lengths and Angles for **7b** and **7d**

bond length/Å	7b	7d	bond angle/deg	7b	7d
Pt(1)–N(1)/Pd(1)–N(1)	2.074(12)	2.088(4)	N(1)–Pd(1)–P(2)/N(1)–Pt(1)–P(2)	90.0(3)	90.55(10)
Pt(1)–Cl(1)/Pd(1)–Cl(1)	2.317(4)	2.3381(12)	N(1)–Pd(1)–P(1)/N(1)–Pt(1)–P(1)	170.6(3)	170.42(10)
Pd(1)–P(1)	2.271(4)	2.701(12)	N(1)–Pd(1)–Cl(1)/N(1)–Pt(1)–Cl(1)	84.3(3)	82.93(10)
Pd(1)–P(2)	2.265(4)	2.2536(11)			

Table 9. Summary of Guest-Trap Abilities of Different Assemblies

	Pt ^{II} (PPh ₃) ₂	Pt ^{II} dppf	Pd ^{II} dppf
isonic		CHCl ₃	CH ₂ Cl ₂ , OTf [−]
Nic	hydrated Na ⁺	CHCl ₃	CHCl ₃
Pic			AgOTf
PyOAc		CHCl ₃	AgOTf
PyPhCO ₂	decomposed		
PyAcr	decomposed		

δ 8.0 (s; pyridyl H), 6.7–7.7 (m; dppf phenyl H), 5.1, 4.8, 4.4, 4.0 (s; dppf Cp H) ppm. ESIMS: *m/z* (%) 1247.71 (100) ([Pd₃-(isonic)₃(OTf)(dppf)₃]²⁺), 83.6 (80) ([Pd(dppf)(isonic)]⁺). IR (KBr): ν 1625 [$\nu_{\text{asym}}(\text{COO})$], 1097 [$\nu_{\text{sym}}(\text{COO})$] cm^{−1}. Anal. Calcd for **1b**·2CHCl₃·2H₂O: C, 42.80; H, 3.17; N, 1.16. Found: C, 43.67; H, 4.99; N, 2.73. Satisfactory elemental analysis could not be obtained because **1b** is highly hygroscopic and inevitably traps air moisture.

Synthesis of [Pd(PyAcr)(dppf)]_n(OTf)_n (2a**).** The preparation of **2a** followed a procedure similar to that of **1b**. A pink solid product was obtained in 80% yield (0.057 g). ³¹P{¹H} NMR: δ 33.3 (b), 36.8 (b) ppm. ¹H NMR: δ 8.6, 8.2, 7.9 (s; pyridyl H), 7.4–7.8 (m; dppf phenyl H), 6.8, 6.9 (s; C=C H), 4.5, 4.6, 4.8, 5.1 (s; dppf Cp H) ppm. ESIMS: *m/z* (%) 809.96 (100) ([Pd(PyAcr)(dppf)]⁺). IR (KBr): ν 1612 [$\nu_{\text{asym}}(\text{COO})$], 1259 [$\nu_{\text{sym}}(\text{COO})$], 2373 [$\nu(\text{C}=\text{C})$] cm^{−1}. Anal. Calcd for **2a**·2CH₂Cl₂: C, 47.92; H, 3.40; N, 1.24. Found: C, 47.68; H, 3.47; N, 1.58.

Synthesis of [Pt(PyAcr)(dppf)]_n(OTf)_n (2b**) and [Pt(dppf)(PyAcrH₂)(OTf)₂ (**3**).** To an aliquot of [Pt(dppf)(MeCN)₂]²⁺ was added PyAcrH (0.0112 g, 0.075 mmol), and the mixture was stirred for 5 h. The mixture was then filtered and the filtrate concentrated to ca. 3 mL. Et₂O was added to afford a yellow precipitate that contained a mixture of **2b** and **3**. This mixture was redissolved in MeOH, and a solution of NH₄PF₆ in MeOH was added. It was then concentrated under vacuum to about of half of its volume and left to stand. The resulting solid deposit was collected by filtration and then redissolved in CH₂Cl₂ and the solution filtered. The filtrate was evaporated to obtain **2b** at 27% yield (0.02 g). Compound **3** was a byproduct, and its pure form could not be obtained. It could be crystallized out in impure form from slow evaporation of a CHCl₃ solution of a mixture of **2b** and **3**. Analysis data for **2b**. ³¹P{¹H} NMR: δ 8.1 (d; *J*_{P–Pt} = 3781 Hz), 5.7 (d; *J*_{P–Pt} = 3488 Hz, ²*J*_{P–P} = 17.4 Hz) ppm. ¹H NMR: δ 8.1, 8.0, 7.9 (s; pyridyl H), 7.2–7.8 (m; dppf phenyl H), 6.4, 5.8 (d; *J* = 15.8 Hz; C=C H), 5.0, 4.7, 4.4, 3.9 (s; dppf Cp H) ppm. ESIMS: *m/z* (%) 897.0 (100) ([Pt(PyAcr)(dppf)]⁺). IR (KBr): ν 1615 [$\nu_{\text{asym}}(\text{COO})$], 1099 [$\nu_{\text{sym}}(\text{COO})$], 2369 [$\nu(\text{C}=\text{C})$] cm^{−1}. Anal. Calcd for **2b**·3CH₂Cl₂: C, 46.41; H, 3.23; N, 1.27. Found: C, 46.25; H, 3.37; N, 1.37.

Synthesis of [Pd(Nic)(dppf)]₃(OTf)₃ (4a**).** The preparation of **4a** was similar to that of **1b**. It was obtained as a pink solid in

83% yield (0.058 g). ³¹P{¹H} NMR: δ 33.6 (b), 39.0 (b) ppm. ¹H NMR: δ 8.8, 8.3, 8.2 (s; pyridyl H), 6.7–7.9 (m; dppf phenyl H), 4.4, 4.7, 4.9, 5.1 (s; dppf Cp H) ppm. ESIMS: *m/z* (%) 781.9 (100) ([Pd(Nic)(dppf)]⁺), 1246.5 (55) ([Pd₃(Nic)₃(OTf)(dppf)₃]²⁺). IR (KBr): ν 1626 [$\nu_{\text{asym}}(\text{COO})$], 1260 [$\nu_{\text{sym}}(\text{COO})$] cm^{−1}. Anal. Calcd for **4a**·7CHCl₃: C, 42.99; H, 2.86; N, 1.16. Found: C, 43.16; H, 3.17; N, 1.92.

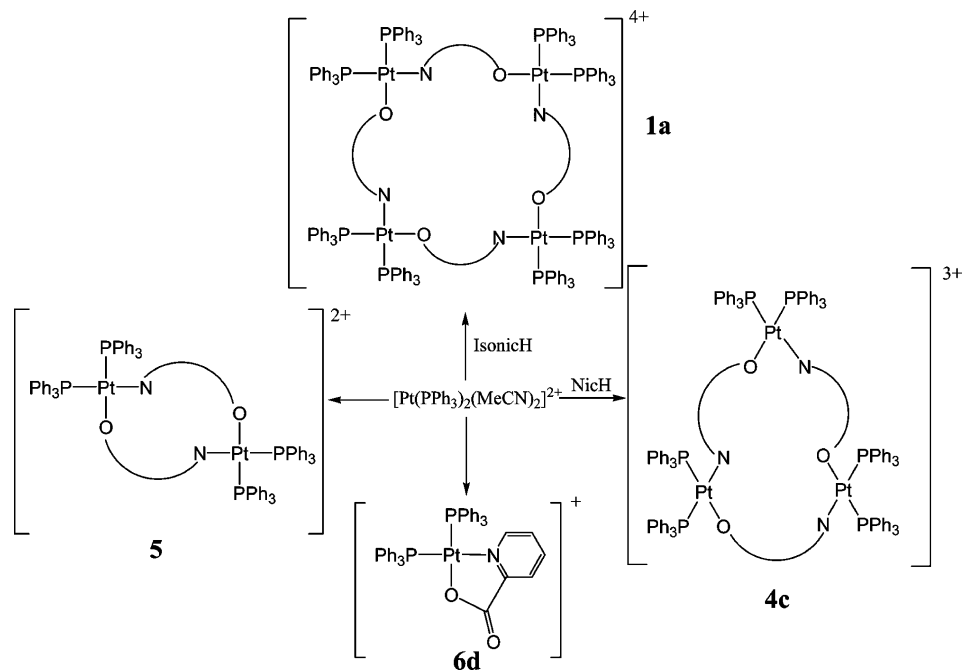
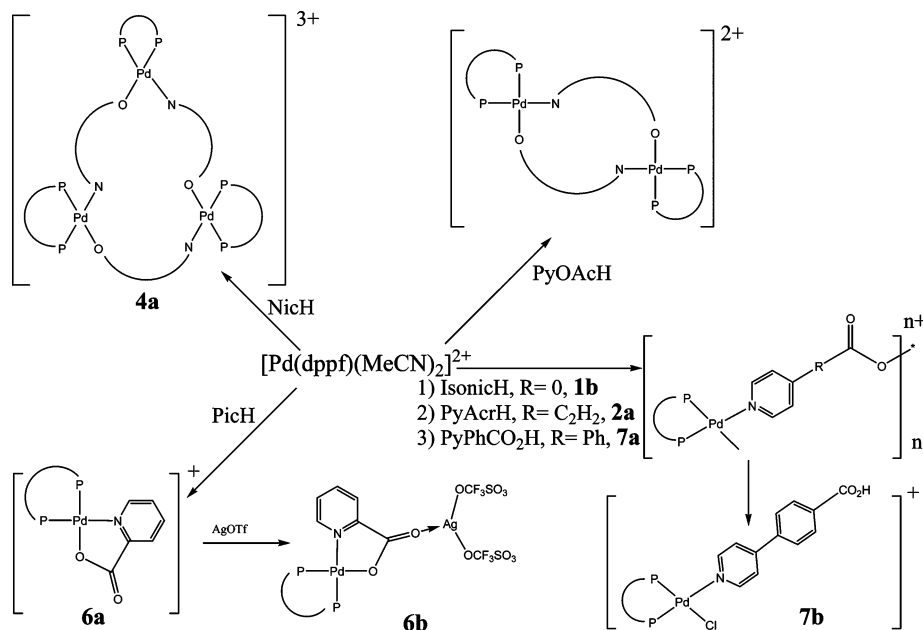
Synthesis of [Pt(Nic)(dppf)]₃(OTf)₃ (4b**).** To an aliquot of [Pt(dppf)(MeCN)₂]²⁺ was added NicH (0.0185 g, 0.15 mmol), and the mixture was stirred for 5 h. The mixture was then filtered and the filtrate concentrated to ca. 3 mL. Et₂O was added to induce precipitation of a yellow solid. The solid was collected by filtration and drying under vacuum to give a yellow solid product at 42% yield (0.032 g). ³¹P{¹H} NMR: δ 8.7 (d; *J*_{P–Pt} = 3779 Hz), 4.5 (d; *J*_{P–Pt} = 3431 Hz, ²*J*_{P–P} = 19.9 Hz) ppm. ¹H NMR: δ 8.9, 8.4, 8.3 (s; pyridyl H), 6.7–7.9 (m; dppf phenyl H), 5.4, 5.0, 4.8, 4.6 (s; dppf Cp H) ppm. ESIMS: *m/z* (%) 871.0 (65) ([Pt(dppf)(Nic)]⁺), 1381.3 (100) ([Pt₃(Nic)₃(OTf)(dppf)₃]²⁺). IR (KBr): ν 1638 [$\nu_{\text{asym}}(\text{COO})$], 1259 [$\nu_{\text{sym}}(\text{COO})$] cm^{−1}. Anal. Calcd for **4b**·4CHCl₃: C, 43.10; H, 2.85; N, 1.19. Found: C, 42.59; H, 3.18; N, 1.45.

Synthesis of [Pt(Nic)(PPh₃)₂]₃(OTf)₃ (4c**).** The preparation of **4c** was similar to that of **1a**. A white solid product was obtained in 80% yield (0.066 g). ³¹P{¹H} NMR: δ 7.3 (d; *J*_{P–Pt} = 3870 Hz), 3.8 (d; *J*_{P–Pt} = 3382 Hz, ²*J*_{P–P} = 22 Hz) ppm. ¹H NMR: δ 8.9 (s; pyridyl H), 6.8–7.6 (m; phenyl H) ppm. ESIMS: *m/z* (%) 1336.99 (100) ([Pt(Nic)(OTf)(PPh₃)₂]⁺), 841.2 (15) ([Pt(Nic)(PPh₃)₂]⁺). IR (KBr): ν 1640 [$\nu_{\text{asym}}(\text{COO})$], 1264 [$\nu_{\text{sym}}(\text{COO})$] cm^{−1}. Anal. Calcd for **4c**·2NaOTf·3CHCl₃·4H₂O: C, 42.95; H, 3.04; N, 1.12; Na, 1.23. Found: C, 42.65; H, 3.16; N, 1.15; Na, 3.85.

Synthesis of [Pt(PyOAc)(PPh₃)₂]₂(PF₆)(OTf) (5**).** AgOTf (0.0530 g, 0.225 mmol) was dissolved in MeCN (5 mL), followed by the addition of CH₂Cl₂ (20 mL). PtCl₂(PPh₃)₂ (0.0593 g, 0.075 mmol) was then added, followed by PyOAc·HCl (0.0130 g, 0.075 mmol). The mixture was stirred for 5 h and filtered. The filtrate was concentrated to ca. 3 mL, and Et₂O was added to afford a white precipitate. The mixture was filtered and the residue redissolved in MeOH. A solution of NH₄PF₆ in MeOH was added and the mixture left to stand overnight, giving a brown precipitate in a colorless solution. The mixture was filtered and the filtrate evaporated to dryness. CH₂Cl₂ was added to extract pure **5** as a white solid at 55% yield (0.041 g). ³¹P{¹H} NMR: δ 6.7 (d; *J*_{P–Pt} = 3731 Hz), 5.7 (*J*_{P–Pt} = 3349 Hz, ²*J*_{P–P} = 22.3 Hz) ppm. ¹H NMR: δ 8.2 (s; pyridyl H), 6.8–7.5 (m; phenyl H), 2.5 (CH₂) ppm. ESIMS: *m/z* (%) 855.19 (100) ([Pt(PyOAc)(PPh₃)₂]⁺), 1854.86 (55) ([Pt(PyOAc)

- (4) (a) Chi, K.; Addicott, C.; Arif, A. M.; Stang, P. J. *J. Am. Chem. Soc.* **2004**, *126*, 16569. (b) Sekiya, R.; Nishikiori, S.; Ogura, K. *Inorg. Chem.* **2006**, *45*, 9233. (c) Crisp, M. G.; Tiekink, E. R. T.; Rendina, L. M. *Inorg. Chem.* **2003**, *42*, 1057. (d) Aakeroy, C. B.; Beatty, A. M.; Leinen, D. S. *Angew. Chem., Int. Ed.* **1999**, *38*, 1815.
- (5) (a) Kubota, Y.; Takata, M.; Matsuda, R.; Kitaura, R.; Kitagawa, S.; Kobayashi, T. C. *Angew. Chem., Int. Ed.* **2006**, *45*, 4932. (b) Kubota, Y.; Takata, M.; Matsuda, R.; Kitaura, R.; Kitagawa, S.; Kato, K.; Sakata, M. *Angew. Chem., Int. Ed.* **2005**, *44*, 920.

- (6) Ghosh, S.; Turner, D. R.; Batten, S. R.; Mukherjee, P. S. *Dalton Trans.* **2007**, 1869.
- (7) Luo, J.; Zhao, Y.; Xu, H.; Kinnibrugh, T. L.; Yang, D.; Timofeeva, T. V.; Daemen, L. L.; Zhang, J.; Thompson, J. D.; Currier, R. P. *Inorg. Chem.* **2007**, *46*, 9021.
- (8) (a) Corain, B.; Longato, B.; Favero, G. *Inorg. Chim. Acta* **1989**, *157*, 259. (b) Jong, F. D.; Bour, J. J.; Schlebos, P. P. *J. Inorg. Chim. Acta* **1988**, *154*, 89.
- (9) Bertani, R.; Michelin, R. A.; Mozzon, M.; Sassi, A.; Basato, M.; Biffis, A.; Martinati, G.; Zecca, M. *Inorg. Chem. Commun.* **2001**, *4* (6), 281.
- (10) *SMART and SAINT Software Reference Manuals*, version 5.611; Bruker Analytical X-ray Systems Inc.: Madison, WI, 2000.
- (11) Sheldrick, G. M. *SADABS software for empirical absorption correction*; University of Göttingen: Göttingen, Germany, 2000.

Scheme 1. Schematic Representation of the Chemical Assembly of Pt^{II}(PPh₃)₂ Squares, Triangles, Rectangles, and Mononuclear Complexes**Scheme 2.** Schematic Representation of the Chemical Assembly of Pd^{II} Triangles, Rectangles, Polymers, and Monometallic Building Blocks

c(OTf)(PPh₃)₂ + H⁺). IR (KBr): ν 1618 [$\nu_{\text{asym}}(\text{COO})$], 1276 [$\nu_{\text{sym}}(\text{COO})$] cm⁻¹. Anal. Calcd for **5**·CHCl₃: C, 49.74; H, 3.46; N, 1.32. Found: C, 50.05; H, 3.68; N, 1.35.

Synthesis of [Pd(Pic)(dppf)](OTf) (6a**).** The preparation of **6a** was similar to that of **1b**. A pink solid product was obtained in 95% yield (0.066 g). ³¹P{¹H} NMR: δ 39.5 (b), 42.5 (b) ppm. ¹H NMR: δ 8.1, 7.9 (s; pyridyl H), 7.0–7.7 (m; dppf phenyl H), 4.3, 4.6 (br s; dppf Cp H) ppm. ESIMS: m/z (%) 782.0 (100) ([Pd(Pic)(dppf)]⁺). IR (KBr): ν 1625 [$\nu_{\text{asym}}(\text{COO})$], 1262 [$\nu_{\text{sym}}(\text{COO})$] cm⁻¹. Anal. Calcd for **6a**·2CH₂Cl₂: C, 46.87; H, 3.29; N, 1.27. Found: C, 46.56; H, 3.27; N, 1.61.

Synthesis of [PdAg(Pic)(OTf)₂(dppf)] (6b**).** Excess AgOTf (0.0579 g, 0.225 mmol) was used in the synthesis of [Pd(dppf)(MeCN)₂]²⁺, followed by the addition of PicH (0.0185 g, 0.15 mmol) to the filtrate of **3**. The rest is the same as that in the synthesis

of **6a**. ³¹P{¹H} NMR: δ 39.5 (b), 42.5 (b) ppm. ¹H NMR: δ 8.1, 7.9 (s; pyridyl H), 7.0–7.7 (m; dppf phenyl H), 4.3, 4.6 (br s; dppf Cp H) ppm. ESIMS: m/z (%) 782.0 (100) ([Pd(Pic)(dppf)]⁺), 1039.3 (10) ([PdAg(Pic)(OTf)(dppf)]⁺). IR (KBr): ν 1655 [$\nu_{\text{asym}}(\text{COO})$], 1164 [$\nu_{\text{sym}}(\text{COO})$] cm⁻¹. This sample of **6b** is invariably contaminated by **6a**, which could not be removed satisfactorily.

Synthesis of [Pt(Pic)(dppf)]OTf (6c**).** The preparation of **6c** was similar to that of **4b**. Yellow solid product was obtained in 90% yield (0.069 g). ³¹P{¹H} NMR: δ 13.1 (d; $J_{\text{P-Pt}} = 3699$ Hz), 9.2 (d; $J_{\text{P-Pt}} = 3731$ Hz, $^2J_{\text{P-P}} = 24.8$ Hz) ppm. ¹H NMR: δ 8.1, 8.0, 7.9 (s; pyridyl H), 7.4–7.8 (m; dppf phenyl H), 4.1, 4.5, 4.6, 4.7 (s; dppf Cp H) ppm. ESIMS: m/z (%) 871.0 (100) ([Pt(Pic)(dppf)]⁺).

(12) *SHELXTL Reference Manual*, version 5.1; Bruker Analytical X-ray Systems Inc.: Madison, WI, 1997.

IR (KBr): ν 1692 [$\nu_{\text{asym}}(\text{COO})$], 1265 [$\nu_{\text{sym}}(\text{COO})$] cm^{-1} . Anal. Calcd for **6c**·2CH₂Cl₂·H₂O: C, 42.73; H, 3.17; N, 1.16. Found: C, 42.40; H, 3.19; N, 1.28.

Synthesis of [Pt(Pic)(PPh₃)₂](OTf) (6d). The preparation of **6d** was similar to that of **1a**. A white solid product was obtained in 85% yield (0.063 g). ³¹P{¹H} NMR: δ 11.2 (d; $J_{\text{P-Pt}} = 3643$ Hz), 6.8 (d; $^1J_{\text{P-Pt}} = 3611$ Hz, $^2J_{\text{P-P}} = 24.8$ Hz) ppm. ¹H NMR: δ 8.2, 8.1 (s; pyridyl H), 7.3–7.5 (m; phenyl H) ppm. ESIMS: m/z (%) 841.1 (100) ([Pt(Pic)(PPh₃)₂]⁺). IR (KBr): ν 1679 [$\nu_{\text{asym}}(\text{COO})$], 1268 [$\nu_{\text{sym}}(\text{COO})$] cm^{-1} . Anal. Calcd for **6d**·CHCl₃: C, 47.60; H, 3.18; N, 1.26. Found: C, 47.07; H, 3.21; N, 1.22.

Synthesis of [Pd(PyBzCO₂)(dppf)]_n(OTf)_n (7a). AgOTf (0.0530 g, 0.225 mmol) was dissolved in MeCN (5 mL), followed by the addition of CH₂Cl₂ (20 mL). PdCl₂(dppf) (0.0549 g, 0.075 mmol) was added, followed by PyBzCO₂H·HCl (0.0177 g, 0.075 mmol). The mixture was stirred overnight and filtered. The filtrate was concentrated to ca. 3 mL, and diethyl ether was added to afford a pink solid. Complex **7a** readily decomposed to red [PdCl(dppf)(PyBzCO₂H)]OTf (**7b**) in the solid state. Analytical results showed a mixture of both **7a** and **7b**. ³¹P{¹H} NMR: δ 33.7, 36.3 (**7a**); 33.1, 38.6 (**7b**) ppm. ¹H NMR: δ 8.8, 8.6, 8.3 (s; pyridyl H), 7.1–8.0 (m; dppf phenyl H and Bz H), 4.5, 4.6, 4.8, 5.1 (s; dppf Cp H) ppm. ESIMS: m/z (%) 860.3 (100) ([Pd(PyBzCO₂)(dppf)]⁺). This sample contains a mixture of **7a** and **7b** and did not give satisfactory IR or microanalytical data.

Synthesis of [Pt(PyBzCO₂)(dppf)]_n(OTf)_n (7c). AgOTf (0.0530 g, 0.225 mmol) was dissolved in MeCN (5 mL), followed by the addition of CH₂Cl₂ (20 mL). PtCl₂(dppf) (0.0549 g, 0.075 mmol) was added, followed by PyBzCO₂H·HCl (0.0177 g, 0.075 mmol). The mixture was stirred for 72 h and filtered. The filtrate was concentrated to ca. 3 mL, and diethyl ether was added to afford a yellow solid. Complex **7c** readily decomposed to orange [PtCl(dppf)(PyBzCO₂H)]OTf (**7d**) in the solid state. Analytical data indicated a mixture of **7c** and **7d**. ³¹P{¹H} NMR: δ 9.0, 6.6 (d; resulting from **7c**), 9.7, 4.5 (s; resulting from **7d**); $J_{\text{P-Pt}} = 4240$, 4218, and 4037 Hz, $^2J_{\text{P-P}} = 17.4$ Hz) ppm. ¹H NMR: δ 8.8, 8.6, 8.3 (s; pyridyl H), 7.1–8.0 (m; dppf phenyl H and Bz H), 4.5, 4.6, 4.8, 5.1 (s; dppf Cp H) ppm. ESIMS: m/z (%) 947.7 (100) ([Pt(PyBzCO₂)(dppf)]⁺). IR (KBr): ν 1617 [$\nu_{\text{asym}}(\text{COO})$], 1099 [$\nu_{\text{sym}}(\text{COO})$] cm^{-1} . Elemental analysis was not performed because it exists as a mixture of **7c** and **7d**.

Crystal Structure Determinations. The diffraction experiments were carried out on a Bruker SMART CCD diffractometer with a Mo K α sealed tube at -50 °C. The program SMART was used for collecting frames of data, indexing reflections, and determining lattice parameters, SAINT for integration of the intensity of reflections and scaling, SADABS for absorption correction, and SHELXTL for space group and structure determination and least-squares refinements on F^2 . The relevant crystallographic data and refinement details are shown in Table 10. For **1a**, the crystal is triclinic, with space group $P\bar{1}$. Solution of the structure showed that the asymmetric unit consists of half of the square cation and only one OTf (instead of two). There were a large number of residual peaks with electron density greater than 2 σ . Of the 11 highest peaks, 9 peaks were assigned as chloroform solvent molecules, one at full occupancy and two at half-occupancy according to thermal parameters. The remaining two peaks were assigned as Cl⁻ at half-occupancy. With this model, the structure refined to $R1 = 0.0703$ and $wR2 = 0.223$ for $2\theta_{\text{max}}$ of 50°. However, there are still many residual peaks that are not identified near the Pt atoms. They could be caused by partially occupied CHCl₃ or water molecules. For **1b**, the crystal structure is monoclinic, with space group $P2(1)/c$. The asymmetric unit consists

of one Pd (with the ligands) and one anion. There is also one water molecule, one nondisordered CHCl₃, and one disordered CHCl₃. Final $R1 = 0.0887$ and $wR2 = 0.2035$ at $2\theta_{\text{max}}$ of 50°. For **2a**, the crystal is monoclinic, with space group Cc . The structure can also be solved in $C2c$ with disorder of the ligand NC₅H₄C₂H₂COO (PyAcr). There were some difficulties in solving the structure, although the space group $C2c$ or Cc appeared to be acceptable and the cationic structure was quite clear. Refinement resulted in poor thermal parameters even for those of the heavy atoms. The dppf group appeared to be disordered. Furthermore, the OTf anion could not be located, except for the S atom. There are also many large residual peaks that had to be fitted as CHCl₃, some of which were disordered or with partial occupancy. The final proposed structure shows that the cation, with a unit of [Pd(PyAcr)(dppf)] linked through the O and N of the ligand to form a zigzag chain. There is one OTf anion per Pd with two and a half CHCl₃ solvent molecules. Final R values for $2\theta_{\text{max}}$ of 50° are $R1 = 0.105$ and $wR2 = 0.2775$. For **3**, the crystal is monoclinic with space group $C2/c$. The asymmetric unit contains half of the complex cation [Pt(PyAcrH)₂(dppf)]²⁺, one OTf anion, and one and a half CHCl₃, with the other half situated at the 2-fold axis. The complete cation can be obtained by generating through the 2-fold axis. Final R values are $R1 = 0.0297$ and $wR2 = 0.0738$. For **4a**, the crystal is isomorphous to that obtained for **4b**, with the Pt atoms in **4b** replaced by Pd. The atoms, including the anions and solvent molecules, occupy similar positions in the unit cell. However, the intensity data quality was poor. Refinement only reached R values of $R1 = 0.16$ and $wR2 = 0.43$. For **4b**, the crystal is triclinic with space group $P\bar{1}$. The asymmetric unit contains one [Pt(Nic)(dppf)]⁺ cation, one OTf anion, two Cl⁻ disordered into four sites, and three and a half CHCl₃. Three OTf anions were expected, but only one could be located. The other two could only be assigned as disordered Cl⁻ in four locations. The half CHCl₃ shares the same position as one of the Cl⁻ ions. Final R values are $R1 = 0.0930$ and $wR2 = 0.277$. R values are relatively high and so is the background noise of the electron map. However, the geometry of the cation appears to be acceptable. For **4c**, the crystal is hexagonal with space group $P6(3)/m$. The asymmetric unit contains one-third of the complex cation [Pt(Nic)(PPh₃)₂]₃, which is a triangle-shaped cation. There should therefore be one OTf anion in the asymmetric unit to balance the charge. However, one and a half OTf anions were found. There were also three chloroform molecules and three water molecules at general or special positions. To account for the missing positive charge, we have assigned one Na (Na1), which is coordinated to OTf and water, and another Na (Na2), which is located at a point of symmetry at special positions. Na2 is disordered (flipped over) and is coordinated with four water molecules. H atoms of the water molecules were not located. Restraints were applied to Na2 and its coordinated O atoms. Final R values are $R1 = 0.0529$ and $wR2 = 0.1342$. For **5**, the crystal is triclinic, with space group $P\bar{1}$. The asymmetric unit contains one complex cation [Pt(PyOAc)(PPh₃)₂]₂, two anions, and some solvent. One of the PPh₃ molecules (P4) is disordered. The three phenyl rings are disordered into two staggered parts. This is necessary because ring L clashes with its symmetry-equivalent part. The two parts therefore have half-occupancy each (parts 1 and 2). As a result of this disorder, one of the two anions had to be disordered too. However, we could not fit two disordered PF₆'s. The best model appeared to be half PF₆ and half OTf because OTf was the original anion used in the preparation of the compound. Together with this disorder, there is also a disordered CHCl₃ in the same part as the PF₆. The model was not perfect, and there are still some residual peaks unaccounted for. However, the model reduced to R values of $R1 = 0.037$ and $wR2 = 0.106$ for $2\theta_{\text{max}}$ of

Table 10. Crystallographic Data for Complexes 1–7^a

	1a	2a	3	4a	4b	4c
empirical formula	C ₁₇₄ H ₁₄₀ Cl ₁₄ F ₆ N ₄ O ₁₄ P ₂ Pd ₄ S ₂	C ₄₂ H _{36.5} Cl _{17.5} F ₃ FeNO ₃ P ₂ PdS	C ₅ H _{4.5} Cl ₉ F ₈ FeN ₂ O ₁₀ P ₂ PdS ₂	C _{124.5} H _{100.5} Cl _{12.5} F ₃ Fe ₃ N ₃ O ₃ P ₆ Pd ₃ S	C ₁₂₄ H _{100.5} Cl _{12.5} F ₃ Fe ₃ N ₃ O ₃ P ₆ Pd ₃ S	C ₁₃₆ H ₁₀₈ Cl ₁₈ F _{13.5} N ₃ Na _{1.5} O ₂₈ P ₆ Pt ₃ S _{4.5}
temperature (K)	223(2)	223(2)	223(2)	223(2)	223(2)	223(2)
fw	4213.44	1256.38	1703.98	2987.33	3253.4	4082.7
cryst syst	triclinic	monoclinic	monoclinic	triclinic	triclinic	hexagonal
space group	P1	C ₂	C ₂ /c	P1	P1	P6(3)/m
unit cell dimens	<i>a</i> (Å) <i>b</i> (Å) <i>c</i> (Å) <i>α</i> (deg) <i>β</i> (deg) <i>γ</i> (deg)	14.8124(5) 14.1690(7) 29.1810(17) 12.3036(7) 90 107.161(2) 90 90 4860.6(5)	20.7213(8) 17.4187(6) 21.1818(8) 90 100.7400(10) 90 90 6442.6(5)	19.1439(18) 19.4624(18) 22.695(2) 95.478(2) 106.696(2) 117.441(2) 6925.1(11)	19.1274(12) 19.4662(12) 22.7920(15) 95.534(2) 106.6190(10) 117.4770(10) 5392.7(3)	22.3917(6) 22.3917(6) 40.7260(17) 90 120 90 17683.8(10)
<i>V</i> (Å ³)	1.297	1.590	1.757	1.433	1.555	1.533
<i>Z</i>	2892	1.081	2.956	1.096	3.694	2.826
<i>D</i> _{calc} (mg/m ³)	2080	2516	3368	3004	3196	8048
abs coeff (mm ⁻¹)	18.974	15.414	22.362	64.830	69.039	102.927
no. of reflns	0.14 × 0.10 × 0.08	0.09 × 0.06 × 0.05	0.30 × 0.20 × 0.15	0.26 × 0.20 × 0.16	0.46 × 0.38 × 0.20	0.42 × 0.22 × 0.20
cryst size (mm ³)	−17 ≤ <i>h</i> ≤ 15	−24 ≤ <i>h</i> ≤ 24	−22 ≤ <i>h</i> ≤ 21	−21 ≤ <i>h</i> ≤ 21	−21 ≤ <i>h</i> ≤ 21	−27 ≤ <i>h</i> ≤ 20
index angles	−22 ≤ <i>k</i> ≤ 21	−20 ≤ <i>k</i> ≤ 17	−16 ≤ <i>k</i> ≤ 23	−22 ≤ <i>k</i> ≤ 22	−22 ≤ <i>k</i> ≤ 22	−27 ≤ <i>k</i> ≤ 27
	−23 ≤ <i>l</i> ≤ 23	−9 ≤ <i>l</i> ≤ 14	−25 ≤ <i>l</i> ≤ 27	−25 ≤ <i>l</i> ≤ 25	−26 ≤ <i>l</i> ≤ 26	−50 ≤ <i>l</i> ≤ 49
R1, wR2(all data)	0.1089, 0.2220	0.1149, 0.2765	0.0341, 0.0742	0.2011, 0.4345	0.1184, 0.2772	0.1249, 0.1539
final R1, wR2	0.0704, 0.1981	0.1050, 0.2661	0.0297, 0.0725	0.1597, 0.4135	0.0930, 0.2580	0.0529, 0.1342
largest diff peak and hole(e ⁻ Å ⁻³)	+1.714 and −0.824	+1.533 and −0.899	+1.140 and −0.787	+5.631 and −1.591	+6.859 and −2.057	+1.282 and −0.700

	5	6a	6b	6c	6d	7a	7b	7c	7d
empirical formula	C ₈₉ H _{74.5} Cl _{7.5} F _{10.5} N ₂ O _{3.5} P ₅ Pt ₅ S _{0.5}	C ₄₂ H _{36.5} Cl _{17.5} F ₃ FeNO ₃ P ₂ PdS	C ₄₃ H ₃₅ AgCl ₃ F ₆ FeNO ₈ P ₂ PdS ₂	C ₄₁ H ₃₂ F ₃ FeNO ₅ P ₂ PS	C ₄₄ H _{33.5} Cl _{4.5} F ₃ N ₃ O ₅ P ₂ PdS	C _{49.5} H _{42.5} Cl _{2.5} F ₃ FeNO _{3.5} P ₂ PdS	C _{50.25} H _{44.75} Cl _{1.75} F ₃ FeNO _{3.75} P ₂ PdS		
temperature (K)	293(2)	293(2)	293(2)	293(2)	293(2)	293(2)	293(2)		
fw	2301.93	1308.23	1308.23	1020.62	1169.85	1141.22	1218.6		
cryst syst	triclinic	monoclinic	triclinic	triclinic	triclinic	triclinic	triclinic		
space group	P1	P2(1)/n	P1	P1	P1	P1	P1		
unit cell dimens	<i>a</i> (Å) <i>b</i> (Å) <i>c</i> (Å) <i>α</i> (deg) <i>β</i> (deg) <i>γ</i> (deg)	11.0226(10) 19.5742(17) 23.097(2) 102.729(2) 103.045(2) 98.305(2) 4635.5(7)	10.5032(4) 15.7460(6) 29.0207(12) 90 99.3330(10) 90 4736.0(3)	10.387(3) 11.925(4) 15.465(5) 90.288(7) 95.555(7) 101.068(7) 1870.5(10)	11.255(2) 12.468(3) 17.168(4) 95.181(4) 102.305(4) 102.492(4) 2274.7(8)	10.221(5) 10.592(5) 22.933(10) 99.443(9) 91.434(10) 98.230(10) 2274.7(8)	10.2832(8) 10.6022(8) 23.0540(18) 99.185(2) 91.459(2) 98.298(2) 2452.2(3)		
<i>V</i> (Å ³)	1.649	1.835	1.835	1.812	1.708	1.566	1.650		
<i>Z</i>	3.410	1.489	4.327	3.523	3.523	0.979	3.409		
<i>D</i> _{calc} (mg/m ³)	2270	2592	2592	1004	1154	1156	1212		
abs coeff (mm ⁻¹)	49.713	33.475	33.475	13.142	30.020	13.206	31.976		
no. of reflns	0.40 × 0.36 × 0.24	0.42 × 0.08 × 0.06	0.42 × 0.08 × 0.06	0.30 × 0.16 × 0.10	0.60 × 0.43 × 0.26	0.26 × 0.10 × 0.08	0.32 × 0.12 × 0.04		
cryst size (mm ³)	−13 ≤ <i>h</i> ≤ 13	−13 ≤ <i>h</i> ≤ 13	−13 ≤ <i>h</i> ≤ 13	−13 ≤ <i>h</i> ≤ 11	−14 ≤ <i>h</i> ≤ 14	−12 ≤ <i>h</i> ≤ 12	−13 ≤ <i>h</i> ≤ 13		
index angles	−23 ≤ <i>k</i> ≤ 23	−20 ≤ <i>k</i> ≤ 14	−20 ≤ <i>k</i> ≤ 14	−16 ≤ <i>k</i> ≤ 16	−16 ≤ <i>k</i> ≤ 16	−12 ≤ <i>k</i> ≤ 12	−13 ≤ <i>k</i> ≤ 13		
	−27 ≤ <i>l</i> ≤ 27	−37 ≤ <i>l</i> ≤ 37	−37 ≤ <i>l</i> ≤ 37	−20 ≤ <i>l</i> ≤ 19	−22 ≤ <i>l</i> ≤ 22	−15 ≤ <i>l</i> ≤ 27	−29 ≤ <i>l</i> ≤ 29		
R1, wR2(all data)	0.0419, 0.1060	0.0907, 0.1640	0.0907, 0.1640	0.0405, 0.0865	0.0366, 0.0793	0.2187, 0.3179	0.0588, 0.0883		
final R1, wR2	0.0372, 0.1024	0.0685, 0.1533	0.0685, 0.1533	0.0355, 0.0839	0.0318, 0.0771	0.1308, 0.2713	0.0426, 0.0833		
largest diff peak and hole(e ⁻ Å ⁻³)	+3.297 and −1.100	+1.762 and −1.248	+1.762 and −1.248	+1.641 and −0.838	+1.508 and −0.736	+2.036 and −1.534	+1.145 and −1.465		

^a The crystal structures have been deposited at the Cambridge Crystallographic Data Centre. CCDC numbers of the complexes: **1a**, 666844; **1b**, 672177; **2a**, 666846; **3**, 666847; **4a**, 666848; **4b**, 666849; **4c**, 666850; **5**, 666851; **6a**, 666852; **6b**, 666853; **6c**, 666854; **6d**, 666854; **7a**, 666855; **7b**, 666855; **7c**, 666856.

50°. No crystal structure was obtained for **6a**. For **6b**, the crystal is monoclinic with space group $P2(1)/n$. The asymmetric unit contains a complex $[\text{PdAg}(\text{Pic})(\text{OTf})_2(\text{dppf})]$. There is also a chloroform solvent molecule that has the C13 disordered into two positions with occupancies of 60:40. Final R values are $R1 = 0.0685$ and $wR2 = 0.1643$. For **6c**, the crystal is triclinic, with space group $P\bar{1}$. In the asymmetric unit, there is one complex $[\text{Pt}(\text{Pic})(\text{dppf})]^+$ cation and one OTf anion. Refinement proceeded to $R1 = 0.05$ and $wR2 = 0.09$, with large residual peaks at C of the OTf as well as small thermal parameters of the C atom. This may be caused by a flip-over disorder of the OTf (i.e., CF_3 and SO_3 exchange positions). A complete disordered model would involve two sets of the OTf and then refinement with the proper geometry and occupancies. This would require extensive restraints on the geometry of the two parts, or else the refinement would not be stable. We have decided on a simple approximate disorder in which the S–C bond of the minor part was included in the refinement. The F and O atoms of the minor part are not included because their positions and thermal parameters would be close to those of the major part. This approximation results in final R values of $R1 = 0.0387$ and $wR2 = 0.0674$ and with no high residual peaks. For **6d**, the crystal is triclinic, with space group $P\bar{1}$. The asymmetric unit contains one cation and half of the solvent CH_2Cl_2 . Final R values are $R1 = 0.0396$ and $wR2 = 0.919$. **7a** rapidly decomposes into **7b** in the solid state; hence, only the crystal structure for **7b** was obtained. For **7b**, the crystal is triclinic, with space group $P\bar{1}$. The asymmetric contains one complex cation $[\text{PdCl}(\text{PyBz-}$

$\text{CO}_2\text{H})(\text{dppf})]^+$ and one OTf anion. There are some residual solvent peaks. These were fitted with partially occupied CHCl_3 and Et_2O (50:50). Restraints in the bond lengths and thermal parameters were applied on these solvent atoms. The intensity data were poor, with $R_{\text{int}} = 0.102$ and $R(\text{sig}) = 0.199$. However, the geometry, bond lengths, and thermal parameters of the cation and anion appeared to be normal. Final R values are high. $R1 = 0.1308$ and $wR2 = 0.0317$ for $2\theta_{\text{max}}$ of 50°. Like in the case of **7a** and **7b**, no crystal was obtained for **7c** because **7c** rapidly decompose to **7d**. For **7d**, the crystal is monoclinic, with space group $P\bar{1}$. In the asymmetric unit, there is one complex cation and one OTf anion. The solvent peaks were fitted with a mixture of Et_2O and CHCl_3 , at an occupancy ratio of approximately 75:25. Final R values are $R1 = 0.0425$ and $wR2 = 0.0889$.

Acknowledgment. We are grateful for financial support from NUS (Grant R143-000-259-112) and A*STAR (Grant R143-000-277-305) and crystallographic assistance from G. K. Tan, as well as for a scholarship from A*STAR for P.T.

Supporting Information Available: X-ray crystallographic data in CIF format. This material is available free of charge via the Internet at <http://pubs.acs.org>.

IC8007238